Stepwise Dynamics of Connecting Filaments Measured in Single Myofibrillar Sarcomeres

Paul Yang, Tsukasa Tameyasu, and Gerald H. Pollack
Department of Bioengineering, University of Washington, Seattle, Washington 98195

ABSTRACT Single relaxed myofibrils of bumblebee flight muscle were subjected to motor-imposed ramp-length changes. The image of the striations was projected onto a linear photodiode array, and sarcomere length was computed as the spacing between centroids of contiguous A-bands. Centroid position was determined by integrating the respective A-band intensity peak and computing the location at which the area on one side was equal to the other. The resulting trace of centroid to centroid span versus time was stepwise, with periods of rapid shortening alternating with periods of pause. An alternative nondiscrete sensor gave similar steps. If thick filament length remains constant, stepwise sarcomere length changes imply that length changes in the connecting filament must be stepwise. Thus, shortening of the connecting filament occurs as a sequence of discrete events rather than as a continuous event.

INTRODUCTION

Understanding of the dynamics of the sarcomere's connecting filament, the titin-containing elastic filament that interconnects the thick filament with the nearest Z-line, was initially based on immunolocalization studies (Wang et al., 1993; Trombitás et al., 1993; Maruyama, 1994; Granzier et al., 1996). From such studies, in combination with mechanical and molecular biological approaches, two likely sites of elasticity have been identified. One is the so-called PEVK domain (Labeit and Kolmerer, 1995; Linke et al., 1996b), which extends upon stretch. Another is the segment of titin that contains long strings of repeating immunoglobulin domains (Labeit and Kolmerer, 1995), which may "superfold" in slack sarcomeres and straighten upon stretch, giving rise to an entropic force (Helmes et al., 1996; Granzier et al., 1996). Either or both may contribute to so-called passive length changes in the sarcomere.

Although stretch of the connecting filament was initially presumed to occur as a smooth, linear function, morphological studies showing that single titin strands contained discrete knoblike elements along their length (Trinick et al., 1984; Maruyama et al., 1984; Wang and Greaser, 1985) implied that length changes might occur discretely. This implication was confirmed in two recent experiments on isolated titin-strand mechanics. Discrete dynamics were demonstrated in AFM experiments which showed that continuous extension of titin produces sawtooth-force records (Rief et al., 1997). And they were observed in optical trap experiments, which showed that after titin-filament stretch, tension relaxation occurred in stepwise fashion (Tskhovrebova et al., 1997). The steps in tension corresponded to length steps on the order of 20 nm.

The possibility that discrete molecular length changes in titin might show up as discrete length changes in the intact sarcomere was first investigated in the mid-1980s in unstimulated single frog muscle fibers (Granzier and Pollack, 1985). When these relaxed fibers were stretched or released, local sarcomere length changes were found to occur in steps. Although the steps were observed by three methods, an aura of skepticism surrounded stepwise measurements in general (see Discussion) and left these results somewhat in abeyance.

For the current experiments we developed a newer method to investigate sarcomere dynamics of considerably smaller samples. The new method allowed us to interrogate single myofibrillar sarcomeres. The results confirm earlier measurements and show with new precision that length changes in unactivated sarcomeres occur in steps comparable to those observed in single titin strands.

METHODS

The experimental preparation and apparatus share many of the same features of single myofibril experiments reported earlier (Bartoo et al., 1993, 1997; Linke et al., 1994, 1996a). Here we summarize the apparatus's main features and focus on those elements unique to these experiments.

Apparatus

The specimen was held in a chamber built on a Zeiss Axiovert-35 inverted microscope. Hydraulic micromanipulators (Narishige) were used to control the respective positions of the two glass needles holding the specimen, one mounted on the tip of a force transducer, the other on a piezoelectric motor. The glass needles were coated with a silicon adhesive (3145 RTV, Dow Corning) to affix the ends of the myofibril. The image of the striations was projected onto a linear photodiode array (Reticon). A 256-diode array was used with the first seven specimens, whereas a 512-diode array was used for the rest. Intensity profile data from the scanned array were fed to a Macintosh Quadra computer and converted to sarcomere length by a custom software program. The computed sarcomere length data were

Received for publication 17 July 1997 and in final form 1 December 1997.

Address reprint requests to Dr. Gerald H. Pollack, Department of Bioengineering, Box 357962, University of Washington, Seattle, WA 98195. Tel.: 206-685-1880; Fax: 206-685-3300; E-mail: pollack@bioeng.washington.edu.

Dr. Tameyasu's present address is Department of Physiology, St. Marianna University, Kawasaki, Japan.

0006-3495/98/03/1473/11 $2.00

transferred to a Power Macintosh (7100/80), which contained a custom LabVIEW application that allowed the step analysis to be performed.

Solutions

The following solutions were used for preparation and experimentation. Rigor solution: 100 mM KCl, 4 mM $MgCl_2$, 4 mM EGTA, and 20 mM imidazole or 3-[*N*-morpholino] propane sulfonic acid (MOPS). Relaxing solution: 100 mM KCl, 4 mM $MgCl_2$, 4 mM EGTA, 4 mM ATP, and 20 mM imidazole or MOPS. Both solutions were at pH 7.0. Glycerol solution: half glycerol and half rigor solution. Triton X-100 relaxing solution: 1% Triton and 99% relaxing solution. Polyethyleneglycol (PEG) solution: 4% PEG in relaxing solution.

Specimens

Bumblebee flight muscles were isolated and refrigerated in 50% glycerol solution overnight and then stored in the freezer at −20°C until just before use. In preparation for the experiment, the glycerinated muscle was immersed in either rigor or relaxing solution for 30–60 min, treated with the 1% Triton X-100 relaxing solution for 1 h, and moved into the relaxing solution for temporary storage.

Then, in a drop of the relaxing solution on a coverslip, the specimen was teased with fine forceps. Because the myofibrils are tightly packed in the bumblebee, it was not easy to isolate a single myofibril directly by this method without inducing overstretch. However, a few single myofibrils were generally isolated by chance, falling naturally or with the aid of forceps to the bottom of the chamber and adhering to the glass surface.

Next the myofibril-containing coverslip was mounted on the stage of the inverted microscope, and a single myofibril was picked up at either end by the two fine glass needles. To ensure firm attachment, the myofibril was wound several times at each end around the tip of the respective glass needle before the glue cured. Usually the segment of myofibril between the two needles contained 50–100 or, occasionally, more sarcomeres. During the preparation process, care was taken not to stretch the myofibril excessively. A representative specimen is shown in Fig. 1.

Protocol

Unless otherwise noted, all experiments were carried out in relaxing solution at room temperature. The solution in the experimental chamber was replaced periodically to avoid condensation of solutes by evaporation and to keep the specimen from heating. Illuminating light was turned to the maximum level only during stretch-release cycles; otherwise, intensity was kept to a minimum. An oil-immersion phase contrast objective (Zeiss, 100×, NA 1.3, oil) was used with no coverslip in the experimental chamber. To optimize the optical conditions, the amount of solution in the chamber was adjusted to produce a flat surface.

Myofibrils with smeared A-bands or severely skewed Z-lines were considered damaged and discarded. In acceptable specimens the Z-line was more or less perpendicular to the myofibril axis at moderate sarcomere length. Stretching frequently but not always caused tilting of Z-lines and A-bands that were otherwise straight. Stretched myofibrils containing some slightly tilted striations were nevertheless used, but care was taken to analyze only the intensity profiles outside these regions.

The bumblebee specimen has extremely narrow I-bands at slack length. Thus a small preliminary stretch was applied to improve the contrast between A- and I-bands and upgrade striation quality. Most measurements were taken above resting length. The stretch-release protocols were then carried out first at relatively short lengths and then at longer lengths. A consistent rate of length change was applied so as to achieve an overall sarcomere length change of ~5% during the release period. For all but the first eight experiments where the rate was twice the value, the nominal rate of release was 0.5%/sarcomere/s. The ramp itself was checked to ensure that it did not introduce any spurious pauses or steps (cf. Blyakhman et al., manuscript submitted for publication; also Fig. 7).

To optimize conditions, the stretch-release cycle was repeated several times before the intensity profiles were recorded. Only if peak-to-valley height did not change appreciably during the stretch-release cycle was the profile accepted. In early experiments (bee 1 to bee 10) the intensity profiles were recorded during the last of such a series of cycles. Thereafter, the intensity profiles were recorded during a single cycle.

Sarcomere length measurement

During the stretch-release cycle, intensity scan data were taken regularly. In the first eight experiments, the sample interval was 31.7 ms, whereas in the remainder it was 62.4 ms. Magnification was 9 pixels/μm. With sarcomere lengths nominally 3 μm, or 25–30 pixels, and scans 512 pixels long, we could capture up to 20 sarcomeres. Essentially, a "movie" of a string of sarcomeres was created (see Fig. 2).

Sarcomere length was defined as the span between the centroids of adjacent A-bands. In the intensity profiles A-bands appear as voltage peaks, I-bands as valleys. The centroid of the A-band was taken as the "center of mass" of the voltage peak, which was calculated by integrating the peak above a threshold and calculating the point at which half the area was on either side. The threshold value was taken to be 5% below the root mean square value of the entire signal. From the analysis above, the length of each sarcomere of the string was recorded with respect to time and was presented as sarcomere length versus time (cf. Fig. 3).

To define a step in the sarcomere length trace, it was necessary to define the pair of pauses surrounding the step. Thus the initial phase of analysis consisted of identifying each pause. Provisionally, a pause was taken as a region of the trace whose estimated best-fit line, by eye, appeared visually

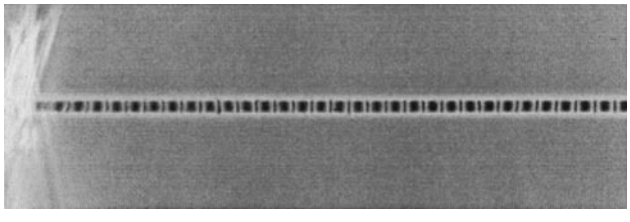

FIGURE 1 Phase-contrast image of representative single myofibril. Attachment point shown at left.

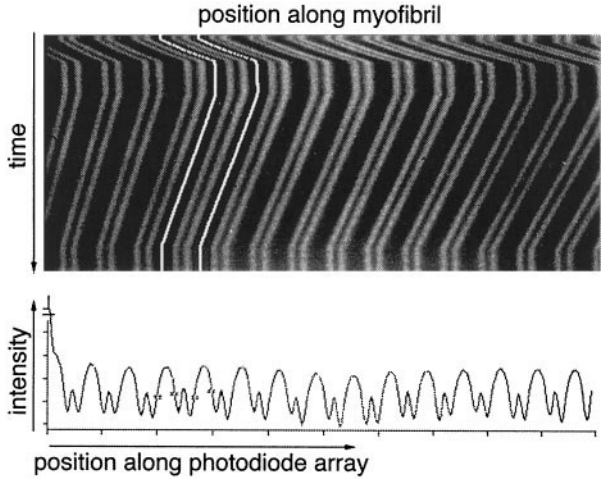

FIGURE 2 (*Top*) Successive scans (*top row to bottom row*) along the myofibril. I-bands are light; A-bands and Z-lines are dark. (*Bottom*) Single scan taken from panel above. A-bands correspond to upward deflections, I-bands to downward deflections. Z-lines are visible as small upward deflections in the middle of each I-band.

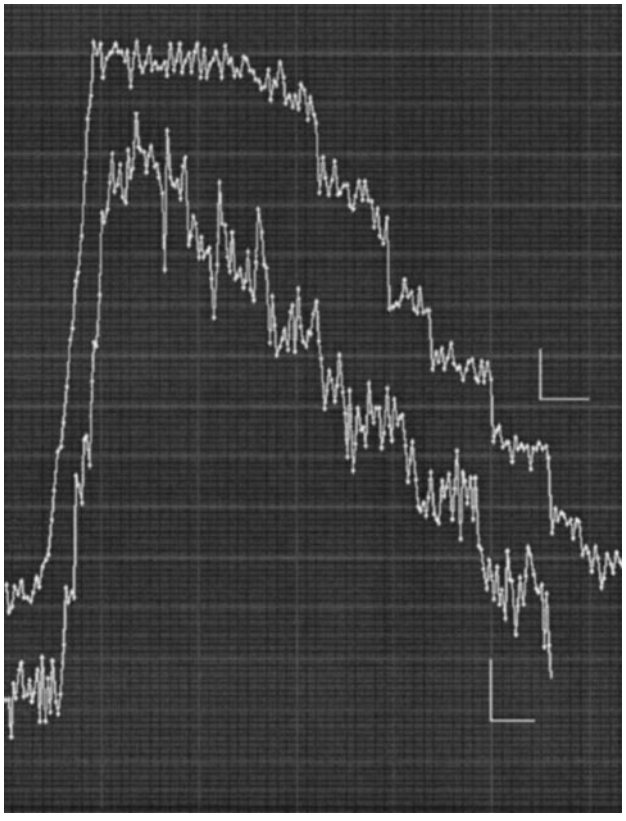

FIGURE 3 Time course of individual sarcomere-length change in two different specimens. Unfiltered data. In each case the motor imposed a rapid stretch-and-hold, followed by slow ramp shortening. Initial sarcomere length: 5.59 μm (*top*), 3.68 μm (*bottom*). Calibration bars: 20 nm; 1 s.

parallel to the horizontal axis. This region had to contain a minimum of three consecutive sample points to qualify.

As the placement of break points could be subjective because of noise, a best-fit line algorithm was applied to allow for more objectivity (cf. Fig. 5). Best-fit lines were computed for the respective pauses and the intervening step. These lines then provided a guide in making the final decision of where to place the break points so as to yield pauses with slope nearest to zero. This iterative process was particularly useful for traces with high noise, but made little difference in traces with low noise, where end points of the pause were unambiguous. Once the best-fit pauses were obtained, the magnitude of the intervening step was calculated by taking the difference of the mean values of the best-fit line segments for the pause preceding and following the step. The entire procedure was then repeated for each step.

To reduce the effect of noise, a median filter was sometimes employed, as noted. The extent of filtering was determined by the filter's rank. Thus a rank n filter takes the running median of every $2n + 1$ points. Filtering with too large a large rank value (>2) degrades the corners that distinguish pauses from steps. Filtering with lower rank values was sometimes effective in eliminating the effect of "outliers."

Alternative sensor

As an alternative to the photodiode array, we implemented a second sarcomere length detector based on a different principle. At the heart of this detector is a galvanometer-based optical scanner (General Scanning G120 DT Closed Loop Scanner) that can cycle up to 300 scans/s, but was used at a rate not exceeding 190 scans/s. The image of the myofibril was magnified by a 100× Ph3 objective and projected initially through a 200-μm-wide slit oriented parallel to the myofibril. This procedure excluded parts of the image external to the myofibril, which would reduce contrast. The myofibril image was then focused onto the surface of the galvanometer mirror. The moving mirror scanned the image across a second slit, 25 μm wide and perpendicular to the myofibril axis. The resulting rectangular image was projected onto a solid-state photomultiplier tube (R5600U; powered by Oriel 70705 at −800 V). The photomultiplier signal was in turn fed to a current-to-voltage converter (gain 10^6), yielding a voltage proportional to local image intensity. The instrument thus yields a scan along the myofibril axis similar to that acquired by the photodiode array, but because this sensor is continuous there is no spatial quantization or "pixelation" of the image. This sensor was used as backup to the photodiode array.

Data processing

Because traces with lowest noise contained distinctly stepwise patterns with rapid steps and zero-slope pauses, we took such patterns as the prototype. Pauses and steps deviating from this standard, whether due to high noise, damaged sarcomeres, slightly skewed A-bands, etc., were accepted into the data set, but could be eliminated based on a set of objective criteria (see Results). These criteria could be applied independently, with threshold values adjusted such that any desired fraction of data could be eliminated.

Statistical analysis was carried out by constructing histograms of step size, with and without application of criteria or filtering. In all, some 491 steps were analyzed with no filter, 932 with rank 1, and 675 with rank 2. The higher count with the rank 1 filter was obtained because more steps could be identified. For rank 2 data still more steps could be identified, but there seemed to be little need to proceed further.

RESULTS

Specimen quality

Fig. 1 shows a phase-contrast image of a representative specimen. The clear striation pattern is typical of insect flight muscles, whose filaments lie in good register. In the bumblebee, myofibril diameter is on the order of 2 μm, twice that of typical vertebrate myofibrils and enough larger to produce superior optical signals. Sarcomere lengths along the specimen are seen to be moderately uniform, but uniformity often tended to decrease somewhat after the specimen was put through multiple stretches and releases.

Repeated scans along the myofibril produced an effective "movie" of the striation pattern. In Fig. 2 the first scan lies at the top. It shows a trace (*left to right*) of several contiguous sarcomeres. Successive scans (*top to bottom*) show how the pattern changes over time. Because the motor, positioned off to the left, is shortening the myofibril and thereby inducing rightward translation, the striation pattern shifts rightward, and then returns. The thin bright traces bisecting two of the A-bands show the computed centroids. The span between adjacent centroids is taken as the sarcomere length.

A single scan of the sequence above is shown at the bottom of Fig. 2. The profile shows distinct A- and I-bands, with Z-lines as small upward blips. The quality of the profile varied with sarcomere length. At natural resting length (~2.7 μm), A/I contrast is weak because I-bands are extremely narrow. As the sarcomere was extended, the

quality increased noticeably. Thus the effective signal-to-noise ratio is higher at longer sarcomere lengths.

Sarcomere dynamics

The time course of single sarcomere length obtained as in Fig. 2 is shown in Fig. 3. In the upper trace the pauses and steps in the shortening pattern are plainly discernible by eye. Pauses persist for up to 1 s or more. Step size is variable, but mainly is on the order of 10–30 nm. In the lower trace, taken from another specimen, the level of noise is higher, but the pauses and steps are nevertheless discernible without filtering. This latter trace also shows pauselike events during the stretch phase, which we observed commonly, but the high motor-stretch speed used in our protocols did not allow for enough samples to be obtained during this phase to enable us to study these putative pauses.

Fig. 4 shows an example in which the steps are marginally discernible in the raw signal (*top trace*). With a rank 1 filter (*middle trace*) several pauses begin to appear, and with a rank 2 filter (*lower trace*) the pauses appear more cleanly. Several short pauselike "glitches" (<150 ms) appear in the signal as well, and whether such glitches are indeed short pauses or arise from residual noise remains uncertain.

Analysis of step size was accomplished as shown in Fig. 5. Each pause was represented by a computed best-fit line segment (see Methods). The step was taken as the vertical span between centers of successive fit segments.

In total, 32 myofibrils were studied and 20 were analyzed for steps. The remaining 12 were not analyzed, either because records were excessively noisy or because erratic shortening traces implied possible damage. From the 20 myofibrils analyzed, we measured a total of 2098 steps comprising filtered and nonfiltered sets.

Step size ranged from 4 nm to more than 50 nm. At the low end, reliability was limited by the noise floor; indeed, some of the shorter pauses and smaller steps are in the same range as the noise (discerned at the top plateau or baseline of each sarcomere length trace), and it is therefore unclear whether such small steps are genuine. At the high end, the results are also influenced by noise, for any genuine pause that is missed because of noise will result in an effectively "double" step. Thus the larger steps could well be a sum of two or more smaller ones. Indeed, with a rank 1 filter applied to reduce noise, we rarely found steps above 30 nm.

One question is the effect of the sensor itself on the waveform. Photodiode array elements are not of absolutely uniform sensitivity, and as the A-band translates along the array it is possible that such nonuniformity generates an artifact. To check this, we repositioned the array between runs (by ~50 pixels) in four experiments so that the striated image fell on a different region of the array. Thus, shorten-

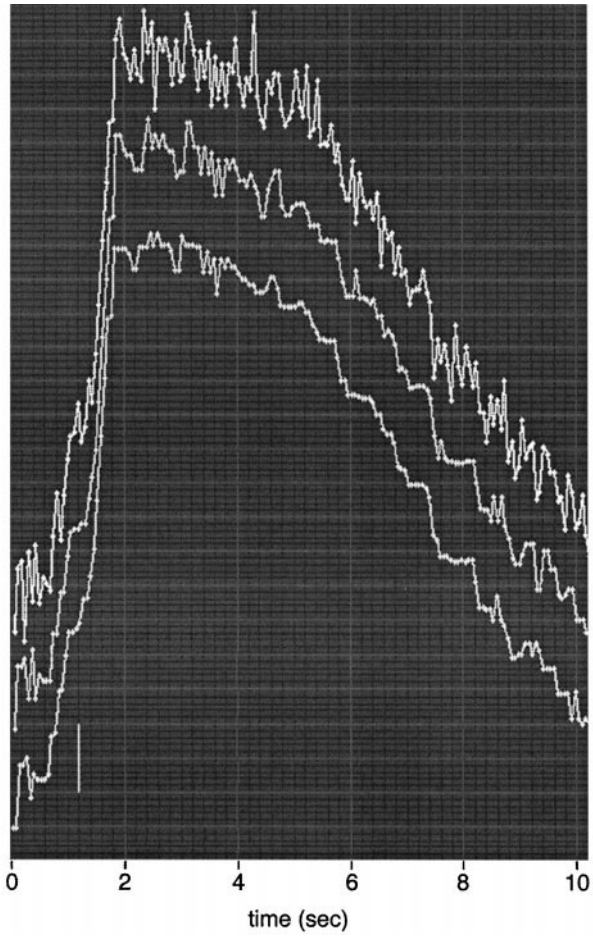

FIGURE 4 Effect of filtering. Format as in Fig. 3, but from another sample. (*Top trace*) Unfiltered; (*middle trace*) rank-1 filter; (*lower trace*) rank-2 filter. Initial sarcomere length 3.87 μm. Calibration bar: 20 nm.

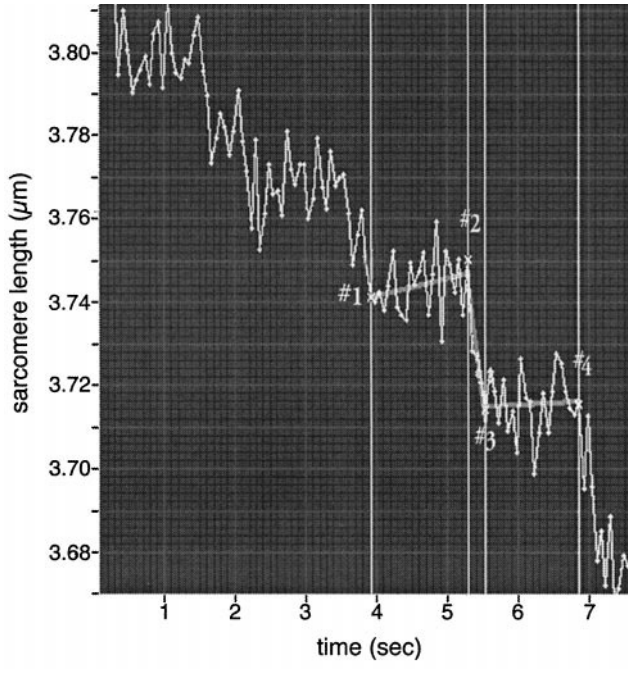

FIGURE 5 Computer analysis of best-fit pauses. Terminal points of each pause (points 1–4) are designated by vertical cursors. Best-fit pause approximations are shown as line segments (1–2 and 3–4) superimposed on the original trace.

ing of the same sarcomere could be checked in two regions of the array. A representative result is shown in Fig. 6 *A*. The same pair of records is shown in Fig. 6 *B* with a rank 2 filter applied. Although top and bottom traces in both panels show some difference, the positioning of the pauses remains essentially the same. The difference is no greater than when successive runs are made in the same region of the array.

Because the array's discreteness is an issue of importance, we carried out another control in which the photodiode array sensor was replaced by a sensor that contained no discrete elements. This sensor consisted of a galvanometer-mirror system that effectively scanned along the myofibril axis and projected the scanned phase image onto a photomultiplier tube (see Methods). The output gave a trace of intensity versus axial position similar in principle to that shown in Fig. 2, except that no discrete sensor was involved.

Representative traces are shown in Fig. 7. The records are of half-sarcomere length (Z-A span) versus time. They are qualitatively similar to those obtained with the photodiode array sensor. Eight myofibrils were studied with this method, and all showed steps of similar nature, although no attempt was made to quantitate the results. To guard against artifact, we measured the time course of translation of smoothly translating objects to see if steps were detectable. The lower records show the computed position of the motor tip and of the A-band closest to the motor, which by virtue of its proximity to the smoothly moving motor, was presumed to translate smoothly as well. No evidence of steps is apparent. The fact that pauses and steps are observed with this nondiscrete sensor implies that the steps do not arise as a consequence of photodiode array discreteness.

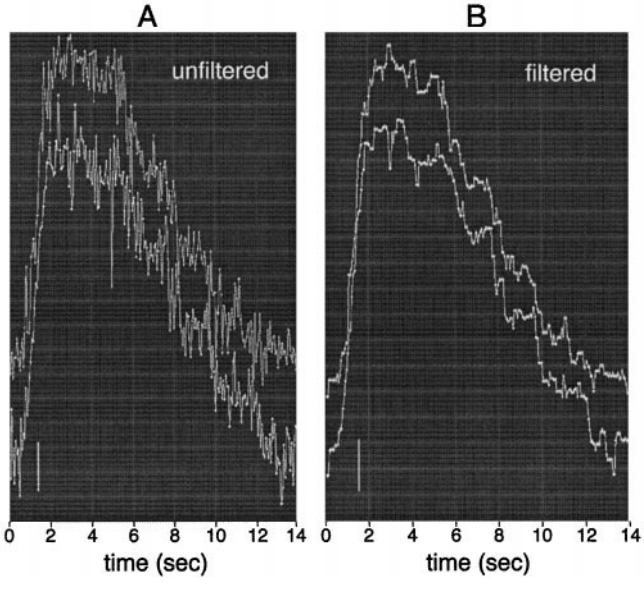

FIGURE 6 Effect of specific photodiode-array elements on the pattern of sarcomere shortening. Top and bottom traces show sarcomere-length computations made when the sarcomere's image fell on different regions of the array. (*A*) Unfiltered; (*B*) rank-2 filter. Initial sarcomere length: 4.53 μm. Calibration bar: 20 nm.

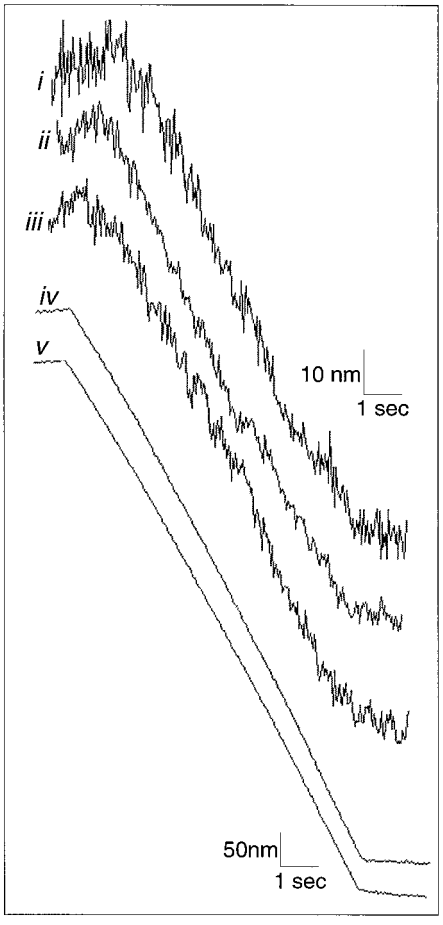

FIGURE 7 Sarcomere length versus time obtained using a scanning-galvanometer mirror and photomultiplier. (*i-iii*) Traces obtained from each of three half-sarcomeres along a myofibril. (*iv* and *v*) Control experiments in the same specimen: translations of motor tip and A-band closest to motor tip are measured as a function of time.

A limited investigation was made of the shortening patterns in contiguous sarcomeres. Because the sum of shortenings of individual sarcomeres is constrained to be smooth by the motor, the timing of steps and pauses cannot be the same in all sarcomeres along the myofibril. Indeed, by examining pairs of traces from contiguous sarcomeres in several specimens, we quickly confirmed this expectation. An example is shown in Fig. 8. Except for seemingly fortuitous coincidence, pauses and steps are not in phase. Such asynchrony was apparently not the case in earlier investigations with larger preparations (e.g., Granzier and Pollack, 1985), where the thousands of series sarcomeres effectively disconnected local behavior from the smooth boundary condition and thereby preserved any existing tendency toward synchrony.

A histogram of step size is shown in Fig. 9. This histogram is the so-called continuous type, which is less susceptible than ordinary histograms to artifactual peaks resulting from the choice of bin size and boundaries. A bin window of 1 nm was selected, and the window was slid along the abscissa by increments of 0.1 nm. At each position the

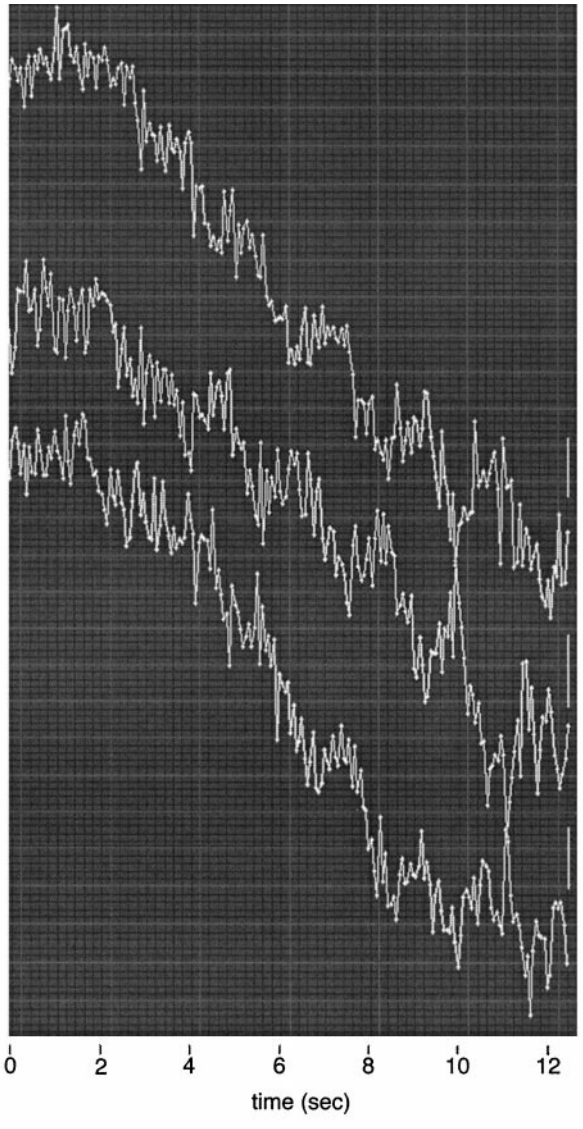

FIGURE 8 Representative example of shortening patterns obtained from three contiguous sarcomeres (*top to bottom*) along the myofibril. Sarcomere lengths (*top to bottom*): 3.70, 3.73, 3.70 μm. Calibration bar: 20 nm.

number of counts within the window was obtained and plotted at the window's center. The window was then slid by 0.1 nm and the calculation was repeated. The resulting histogram was essentially similar to that obtained with the discrete histogram (Fig. 9, *inset*), but for some details. The histograms of Fig. 9 were obtained from unfiltered data.

An interesting feature of the histogram is its peaked, or spiky, nature. The peaks indicate a preference for certain step sizes over others. In the histogram of Fig. 9 the peaks are spaced with moderate regularity, and a least-squares-fit algorithm chose 2.46 nm as the optimum separation. The multipeaked nature of such histograms in activated specimens is dealt with in detail elsewhere (Blyakhman et al., manuscript submitted for publication).

Apart from its multipeaked nature, the histogram shows a broad distribution of step size ranging from several nanometers to beyond 40 nm. There is some hint of a depression near the middle, in the range of 16–20 nm, although this feature is uncertain. It may be that a cluster of "primary" points lies in the range of 8–15 nm, with a secondary cluster, 22–35 nm, reflecting the double steps mentioned above.

To minimize subjectivity of the results, we imposed objective criteria on the selection of pauses and steps. Representative results are shown in Fig. 10. Criteria were imposed on: the step, whose steepness had to exceed a given threshold (Fig. 10 *A*); the pause, whose flatness could not deviate by more than a selected amount from zero (Fig. 10 *B*); and the noise, whose mean square error relative to the best fit had to lie within a threshold (Fig. 10 *C*). In each case, the threshold was arbitrarily selected so as to eliminate ~20% of data points.

Different criteria had different effects on the histogram. The step slope criterion tended to eliminate mainly the larger steps (Fig. 10 *A*), including those whose course may have been slowed by the presence of undetected short pauses. The pause-flatness criterion eliminated some mid-value steps (Fig. 10 *B*): smaller steps were obtainable only from the highest quality records and were thereby unaffected by the application of criteria, and high-end steps were generally associated with long pauses, the slope of which could be confidently determined visually as being near zero and again as being unaffected by application of this criterion. The mean-square-error noise criterion was perhaps the most "useful" (Fig. 10 *C*), in that individual peaks were sharpened. The overall shape of the histogram, however, remained fairly consistent, irrespective of the criterion.

DISCUSSION

The principal result is that the pattern of shortening in relaxed single sarcomeres was found to be stepwise. The implication, if the result is genuine, is that the connecting filament must itself have changed in length of steps—a feature that has already been confirmed during the stretch of isolated titin strands (Rief et al., 1997; Tskhovrebova et al., 1997). A secondary implication arises from the unusual character of the step-size distribution, which offers a clue to the underlying mechanism.

Potential artifacts

The most serious concern is the possibility of instrument artifact. Notwithstanding the isolated titin steps, the sarcomere length change might in fact be smooth, with the steps arising out of some unexpected feature of the apparatus.

The most obvious source of artifact is sensor discreteness. During sarcomere shortening, the A-bands translate along the photodiode array, and it is possible that as the sarcomeric image passes from one photodiode to another, some discreteness is induced in the signal, which appears as steps. This type of artifact implies a step for every photodiode

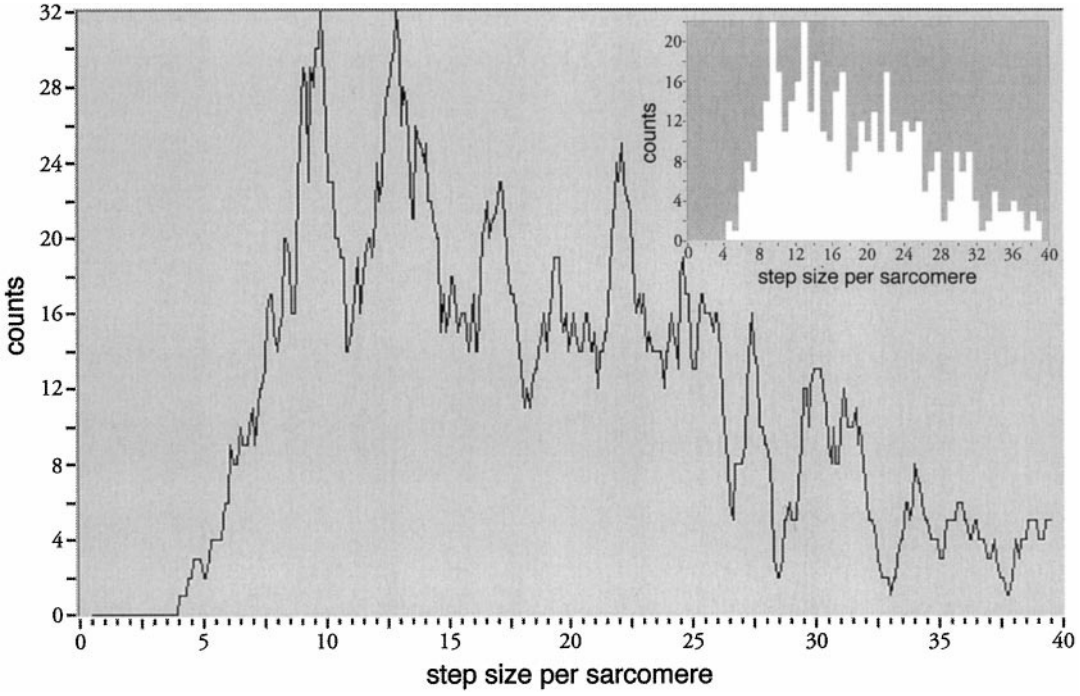

FIGURE 9 Histogram of step size. See text for details. (*Inset*) Same data plotted as a discrete histogram with 1-nm bin width.

traversed. However, the sarcomere typically occupied 30 photodiodes, and shortening by only a few percent (less than one photodiode) could produce a long cascade of steps. For sarcomeres near the myofibril's fixed end, where axial translation is minimal, a 10-nm step would result in translation of less than 0.1 photodiode. Thus the possibility that the step might be caused by translation is quantitatively inconsistent.

A closely related possibility is that the step arises out of defects in certain elements of the array. This was tested by shifting the array so that the sarcomeric image fell on one or another region along the array, where the anticipated defects would be different. The shortening traces were essentially similar (Fig. 6).

We also tested for general photodiode-array artifacts, including translation by substituting a sensor that involved no discrete elements. A simple scanning galvanometer mirror and photomultiplier gave a result similar to that of the photodiode array (Fig. 7).

Another possibility is that the steps arise out of some problem with the software used to convert the striation pattern into sarcomere length. However, essentially similar results were obtained with an independent software package rewritten in LabVIEW and reported elsewhere (Blyakhman et al., manuscript submitted for publication). The latter study also includes several additional controls: a test for motor-induced steps by recording motor movement at high resolution; a test for translation artifacts by measuring translation of the A-band nearest the smoothly moving motor; and a test for systematic artifacts by recording the striation pattern at two different magnifications. All controls proved satisfactory. Thus, the results of this parallel study failed to detect any defect in the software or in the photodiode array that could have given rise to the steps.

Relation to previous work

The present work is not the first report of stepwise shortening in muscle; it is the first report of stepwise shortening in the single sarcomere. Earlier reports of stepwise shortening were based on experiments on larger scale preparations. Initial experiments employed the three following methods: optical diffraction (Pollack et al., 1977); high-speed cinematography (Delay et al., 1981); and phase-locked loop analysis of the striations (Jacobson et al., 1983). All of these methods have been extensively criticized, largely because of their susceptibility to translation artifacts (Huxley, 1984, 1986; Altringham et al., 1984) and because of complexities of interpretation of the optical diffraction signal (Rüdel and Zite-Ferenczy, 1979; Goldman and Simmons, 1984; Huxley, 1984; Sundell et al., 1986; Goldman, 1987). Although such potential artifacts are demonstrably capable of appreciable signal contamination, we have presented evidence that they cannot be responsible for the ultimate presence of steps (Pollack, 1984; Pollack et al., 1979, 1984, 1988). Controversy over the validity of these early methods continues (Burton and Huxley, 1995).

In response to the controversy, we and others developed alternative methods. In one approach we used a segment-length method based on the span between surface markers (Granzier et al., 1987). In another approach we directly

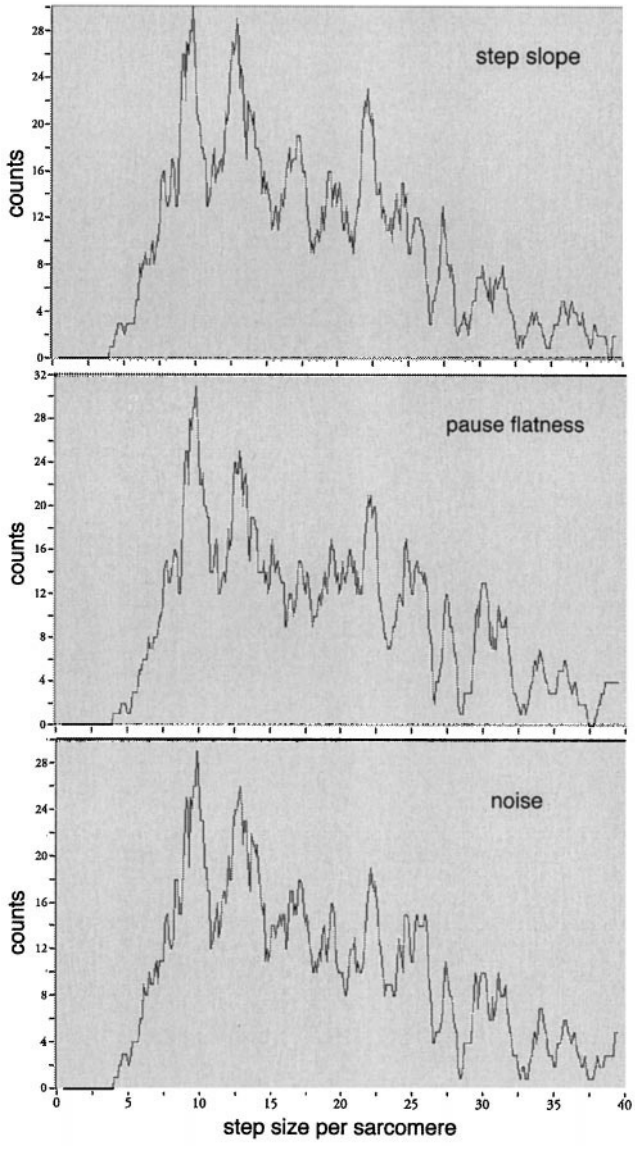

FIGURE 10 Effect of imposing objective criteria on the selection of steps. See text for explanation.

measured the shortening of the end of the fiber (Granzier et al., 1990). Extensive controls were carried out, including controls for specimen translation, and both methods showed clear stepwise shortening. Stepwise shortening was also confirmed by Tameyasu et al. (1985), who measured the spacing between natural markers in single cardiac cells. It was confirmed by Toride and Sugi (1989), who used high-speed cinematography to track length changes of a consistent, nontranslating set of sarcomeres. And it was confirmed again by Tameyasu (1994), who used a scanning mirror system to track sarcomere length changes. To our knowledge, none of these results has been challenged—neither the reports from our laboratory nor those from the other laboratories.

Of particular relevance here is the report of stepwise shortening in unstimulated single frog fibers. This was observed by three methods: optical diffraction, the phase-locked loop sensor, and the surface marker method (Granzier and Pollack, 1985). The fact that the steps could be observed beyond thick-thin filament overlap implied that their origin lay in the connecting filament. A notable feature of the results was the nature of the step-size histogram, which was remarkably similar to that reported here, lower resolution notwithstanding. Both histograms extended at the low end down to ~5 nm, and both showed multiple peaks separated by 2–3 nm. The instrumentation and analytical procedures were entirely independent. In essence, then, the newer results serve largely to confirm that the observations made initially on large preparations apply also to the single sarcomere.

Synchrony

An interesting implication of the single sarcomere measurements is that shortening events seem to occur synchronously over the myofibrillar cross section; otherwise the steps would not be observable. The cross section may contain some 10^3 connecting filaments, and if most or all filaments did not step simultaneously, the shortening trace would be smooth. One explanation of cross-sectional synchrony may lie in the I-band struts that cross-link filaments. These struts are particularly distinct in insect flight muscles (overstretched to prevent thin filaments from complicating the image), where they are detectable not only in thin electron microscopic sections, but also by freeze fracture (Trombitás et al., 1988; Pollack, 1990b). Thick and connecting filaments are also laterally connected at M- and Z-lines, respectively. By linking parallel filaments, these struts, together with M- and Z-line linkages, may constrain the ensemble to step in unison. Thus, synchronized length steps would be evident in the whole sarcomere. Given the whole-sarcomere expression of small length steps, the implication is that these lateral connections are quite stiff. On the other hand, nanometer-scale steps are also observed during unfolding of albumin molecules (Zocchi, 1997), where no struts are available to synchronize the <100 molecules that are observed to step synchronously. Thus, some other mechanism may underlie synchronization, with the struts playing perhaps a secondary role.

Prominent struts also link adjacent myofibrils at both the M- and Z-lines (Pollack, 1990b, p. 152). This feature may help explain the global synchrony implied by the above-mentioned step measurements in larger preparations.

Character of steps

The range of step size in the single sarcomere was broad, with typical values on the order of 10–20 nm. If these sarcomere steps occurred synchronously in constituent half-sarcomeres, then the step per half-sarcomere would be half this value, or 5–10 nm. Otherwise, the value per half-sarcomere is the 10–20-nm figure. Because the algorithm

did not allow us to measure the length of the half-sarcomere, we were unable to distinguish these possibilities in this study. However, a newer algorithm that does allow half-sarcomere measurements to be made shows at least in the activated state that complementary half-sarcomeres step nonsynchronously (Blyakhman et al., manuscript submitted for publication). If true as well in unactivated sarcomeres, as preliminary evidence with the scanning-galvanometer mirror sensor implies, then the step values reported here apply to the half-sarcomere.

In addition to the preponderance of steps in the 10–20-nm range, we also found considerably larger steps. These latter steps could reflect molecular shortening events of large size, but more likely they reflect a limitation imposed by noise. In the presence of noise, short pauses may go undetected, and if so the measured step would be a sum of two or more closely serial steps. Thus the higher the noise, the more likely it is for larger steps to be reported. We found that by filtering the records (rank 1 or rank 2), pauses that were otherwise undetectably short became apparent (cf. Fig. 4). These smaller steps shifted the histogram's center of gravity leftward. Thus, little significance should be attributed to the precise location of the histogram's center of gravity; that depends on the quality of the original signals.

In this connection it is interesting to compare the step size measured in this study during elastic shortening of intact sarcomeres with the steps measured on single titin molecules (Tskhovrebova et al., 1997). In that study the size distribution extended from 5 nm up to ~50 nm, similar to our result (Fig. 9). The most frequent step size in that study was 10–15 nm, also similar to our finding (Fig. 9). Considering that protein isoforms are not the same in the two cases, and considering the inevitable experimental errors, the similarity of the respective size distributions is impressive and implies that the two approaches are likely to be revealing the same phenomenon.

It bears emphasizing, however, how the measured in situ elastic behavior of whole sarcomeres differs from that of the single molecule. Rief et al. (1997) could detect discrete length changes during stretch, but tried and failed to detect stepwise components during shortening phase of stretch-relaxation cycles (their Fig. 4). By contrast, steps in the intact sarcomere appear during both shortening (this paper) and stretch (Tourovskaya and Pollack, 1998). The reason for these differences is unclear, but may lie in the steric constraints absent from the isolated molecule but present in the intact sarcomere.

Origin of steps

Unless thick filaments changed length, it seems inescapable that the stepwise sarcomere length changes observed here imply stepwise connecting filament length changes. This conclusion does not imply that the connecting filament is necessarily the steps' source. The steps could conceivably arise from thin-thick filament interaction, which may persist even in relaxed specimens, or from connecting filament–thin filament interaction. As for the former, some of the experiments were carried out at lengths where the sarcomere was stretched beyond thick-thin filament overlap (>4.5 μm) and the steps were equally clear (see also Granzier and Pollack, 1985). As for connecting-thin interaction, we have found clear steps in sarcomeres stretched such that the thin filaments broke from the Z-line, leaving the connecting filaments as the sole force-bearing element in the I-band (unpublished observations). Thus some feature of the connecting filament itself seems capable of generating steps, and this is supported by the above-mentioned work on single titin filaments (Tskhovrebova et al., 1997; Rief et al., 1997), although the titin steps were not detected during shortening but only during lengthening.

One caveat regarding extrapolation of any titin results to our work is that although titin may be the principal protein (although not necessarily the sole protein; cf. Pollack, 1990b) in vertebrate connecting filaments, it is not necessarily the major protein in insect flight muscle. Titin's presence in flight muscles, including those of the bee, has been demonstrated by immunolabeling (Hu et al., 1990). And gels of insect flight muscle show a protein about the same size as titin (Bullard and Leonard, 1996). But additional proteins are also abundantly present. One protein is projectin (also called mini-titin), which has a titin-like appearance when examined by rotary shadowing, but is shorter than titin (Nave and Weber, 1990). Another protein is kettin, which is mainly a Z-line protein, but projects somewhat into the I-band (Lakey et al., 1990, 1993). Both projectin and kettin have much the same modular structure as titin (and twitchin), with repeating immunoglobulin-like (kettin) and immunoglobulin and fibronectin-like (projectin) domains (Bullard and Leonard, 1996). Thus clear differences exist between vertebrate and insect flight muscle connecting filament proteins, even if the steps in all of these proteins arise from the same modules.

If a common module is responsible, that module may well be the immunoglobulin domain. This domain repeats multiple times in each of the above-mentioned connecting filament proteins, and particularly in the I-band region of titin. In the study by Rief et al. (1997), experiments on recombinant titin-immunoglobulin segments of different lengths showed that the number of discrete events never exceeded the number of immunoglobulin domains, which led them to conclude that discreteness lay in an unfolding of individual immunoglobulin domains. This does not necessarily imply that other regions, such as the so-called PEVK region (Labeit and Kolmerer, 1995) or the fibronectin-like domains in the A-band, could not give rise to steps, but the data of Reif et al. confirm that the presence of immunoglobulin domains is sufficient to obtain the steps.

The interesting question is why the steps measured here (also in the study of Tskhovrebova et al.) are as variable in size as they are. Variability could be explained, at least to some extent, if each domain type gave rise to a characteristic size. An interesting alternative arises from the multi-

peaked nature of the size histogram we obtained (Figs. 9 and 10). Although the peaks are not spaced with precise regularity, some degree of regularity is apparent. A least-squares algorithm similar to the one used by Millikan (1947) to ascertain whether the charge on the electron was quantal, gave a best-fit value of 2.46 nm as the spacing between peaks. Thus step size may take on preferred values that are approximately integer multiples of 2–3 nm. If the shortening steps arise from folding of the immunoglobulin domain, then the results imply that fold increments on the order or 2–3 nm may be detectable.

The immunoglobulin domain of titin has a typical sevenfold antiparallel β-sheet structure (cf. Erickson, 1994; Improta et al., 1996). Each domain contains ~90 residues. Thus each turn is several nanometers in length. Depending on the extent and straightness of the unfolded chain (Kellermayer et al., 1997), the length difference between the folded and unfolded states will have increments on the order of several nanometers. Thus an interesting possibility worthy of followup is that the 2–3-nm increments reflect the foldings of individual turns of the β-sheet. Folding would then be complete at seven times this increment or roughly 7×2.46 nm = 17 nm, and it is at about this value that the histograms show a dip (Fig. 9 and 10).

We thank Dr. R. C. Jacobson for many helpful suggestions regarding the analytical procedures; Anna Tourovskaia for help with data analysis; and John Myers, Jeff Magula, and Mark Fauver for excellent technical assistance.

REFERENCES

Altringham, J. D., R. Bottinelli, and J. W. L. Lacktis. 1984. Is stepwise sarcomere shortening an artifact? *Nature.* 307:653–655.

Bartoo, M. L., W. A. Linke, and G. H. Pollack. 1997. Basis of passive tension and stiffness in isolated rabbit myofibrils. *Am. J. Physiol.* 273: C266–276.

Bartoo, M. L., V. I. Popov, L. Fearn, and G. H. Pollack. 1993. Active tension generation in isolated skeletal myofibrils. *J. Muscle Res. Cell Motil.* 14:498–510.

Bullard, B., and K. Leonard. 1996. Modular proteins of insect muscle. *Adv. Biophys.* 33:211–221.

Burton, K., and H. F. Huxley. 1995. Identification of source of oscillations in apparent sarcomere length measured by laser diffraction. *Biophys. J.* 68:2429–2443.

Delay, M. J., N. Ishide, R. C. Jacobsen, G. H. Pollack, and R. Tirosh. 1981. Stepwise sarcomere shortening: analysis by high-speed cinemicrography. *Science.* 213:1523–1525.

Erickson, H. P. 1994. Reversible unfolding of fibronectin type III and immunoglobulin domains provides the structural basis for stretch and elasticity of titin and fibronectin. *Proc. Natl. Acad. Sci. USA.* 91: 10114–10118.

Goldman, Y. E. 1987. Measurement of sarcomere shortening in skinned fibers from frog muscle by white light diffraction. *Biophys. J.* 52:57–68.

Goldman, Y. E., and R. M. Simmons. 1984. Control of sarcomere length in skinned muscle fibres of *Rana temporia* during mechanical transients. *J. Physiol. (Lond.).* 184:497–518.

Granzier, H. L. M., M. Helmes, and K. Trombitás. 1996. Nonuniform elasticity of titin in cardiac myocytes: a study using immunoelectron microscopy and cellular mechanics. *Biophys. J.* 70:430–442.

Granzier, H. L. M., A. Mattiazzi, and G. H. Pollack. 1990. Sarcomere dynamics during isotonic velocity transients in single frog muscle fibers. *Am. J. Physiol.* 259:C266–C278.

Granzier, H. L. M., J. A. Myers, and G. H. Pollack. 1987. Stepwise shortening of muscle fiber segments. *J. Muscle Res. Cell Motil.* 8:242–251.

Granzier, H. L. M., and G. H. Pollack. 1985. Stepwise shortening in unstimulated frog skeletal muscle fibers. *J. Physiol. (Lond.).* 362: 173–188.

Helmes, M., K. Trombitas, and H. Granzier. 1996. Titin develops restoring force in rat cardiac myocytes. *Circ. Res.* 79:620–627.

Hu, D., A. Matsuno, K. Terakado, T. Matsuura, S. Kimura, and K. Maruyama. 1990. Projectin is an invertabrate connectin (titin): isolation from crawfish claw muscle and insect flight muscle. *J. Muscle Res. Cell Motil.* 11:497–511.

Huxley, A. F. 1984. Response to "Is stepwise shortening an artifact?" *Nature.* 309:713–714.

Huxley, A. F. 1986. Comments on "Quantal mechanics in cardiac contraction." *Circ. Res.* 59:9–14.

Improta, S., A. S. Politou, and A. Pastore. 1996. Immunoglobulin-like modules from titin I-band: extensible components of muscle elasticity. *Structure.* 4:323–337.

Jacobson, R. C., R. Tirosh, M. J. Delay, and G. H. Pollack. 1983. Quantized nature of sarcomere shortening steps. *J. Muscle Res. Cell Motil.* 4:529–542.

Kellermayer, M. S. Z., S. B. Smith, H. L. Granzier, and C. Bustamante. 1997. Folding-unfolding transitions in single titin molecules characterized with laser tweezers. *Science.* 276:1112–1116.

Labeit, S., and B. Kolmerer. 1995. Titins: giant proteins in charge of muscle ultrastructure and elasticity. *Science.* 270:293–296.

Lakey, A., C. Ferguson, S. Labeit, M. Reedy, A. Larkins, G. Butcher, K. Leonard, and B. Bullard. 1990. Identification and localization of high molecular weight proteins in insect flight and leg muscle. *EMBO J.* 9:3459–3467.

Lakey, A., S. Labeit, M. Gautel, C. Ferguson, D. Barlow, K. Leonard, and B. Bullard. 1993. Kettin, a large modular protein in the Z-disc of insect muscles. *EMBO J.* 12:2863–2871.

Linke, W. A., M. Ivemeyer, M. L. Bartoo, and G. H. Pollack. 1996a. Limits of titin extension in single cardiac myofibrils. *J. Muscle Res. Cell Motil.* 17:425–438.

Linke, W., M. Ivemeyer, N. Olivieri, B. Kolmerer, J. Ruegg, and S. Labeit. 1996b. Towards a molecular understanding of the elasticity of titin. *J. Mol. Biol.* 261:62–71.

Linke, W. A., V. I. Popov, and G. H. Pollack. 1994. Passive and active tension in single cardiac myofibrils. *Biophys. J.* 67:782–792.

Maruyama, K. 1994. Connectin, an elastic protein of striated muscle. *Biophys. Chem.* 50:73–85.

Maruyama, K., Y. Toshitada, H. Yoshidomi, H. Sawada, and M. Kikuchi. 1984. Molecular size, and shape of β-connectin, an elastic protein of striated muscle. *J. Biochem.* 95:1423–1493.

Millikan, R. A. 1947. Electrons (+ and −), Protons, Photons, Neutrons, Mesotrons, and Cosmic Rays, 2nd Ed. University of Chicago Press, Chicago.

Nave, R., and K. Weber. 1990. A myofibrillar protein of insect muscle realted to vertabrate titin connects Z band and A band: purification and molecular characterization of invertabrate mini-titin. *J. Cell Sci.* 95: 535–544.

Pollack, G. H. 1984. Is stepwise shortening an artifact? A response. *Nature.* 309:712–714.

Pollack, G. H. 1990a. Optical scattering studies of muscle contraction. *In* Noninvasive Techniques in Cell Biology. S. Grinstein, editor. Wiley-Liss, New York. 311–326.

Pollack, G. H. 1990b. Muscles and Molecules: Uncovering the Principles of Biological Motion. Ebner and Sons, Seattle, WA.

Pollack, G. H., H. L. M. Granzier, A. Mattiazzi, C. Trombitas, A. Periasamy, P. H. W. W. Baatsen, and D. H. Burns. 1988. Pauses, steps, and the mechanism of contraction. *In* Molecular Mechanism of Muscle Contraction. H. Sugi and G. H. Pollack, eds. Plenum Press, New York. 617–637.

Pollack, G. H., T. Iwazumi, H. E. D. J. ter Keurs, and E. F. Shibata. 1977. Sarcomere shortening in striated muscle occurs in stepwise fashion. *Nature.* 268:757–759.

Pollack, G. H., R. Tirosh, F. V. Brozovich, J. W. Lacktis, R. C. Jacobson, and T. Tameyasu. 1984. Stepwise shortening: evidence and implications. *In* Contractile Mechanisms in Muscle. G. H. Pollack and H. Sugi, eds. Plenum Press, New York. 765–786.

Pollack, G. H., D. V. Vassallo, R. C. Jacobson, T. Iwazumi, and M. J. Delay. 1979. Discrete nature of sarcomere shortening in striated muscle. *In* Cross-Bridge Mechanisms in Muscle Contraction. H. Sugi and G. H. Pollack, eds. University of Tokyo Press, Tokyo. 23–40.

Rief, M., M. Gautel, F. Oesterhelt, J.Fernandez, and H. E. Gaub. 1997. Reversible unfolding of individual titin immunoglobulin domains by AFM. *Science.* 276:1109–1112.

Rüdel, R., and F. Zite-Frenczy. 1979. Do laser diffraction studies on striated muscle indicate stepwise sarcomere shortening? *Nature.* 278: 573–575.

Sundell, C., Y. Goldman, and L. Peachey. 1986. Fine structure in near-field and far-field laser diffraction patterns from skeletal muscle fibers. *Biophys. J.* 49:521–530.

Tameyasu, T. 1994. Oscillatory contraction of single sarcomere in single myofibril of glycerinated, striated adductor muscle of scallop. *Jpn. J. Physiol.* 44:295–318.

Tameyasu, T., T. Toyoki, and H. Sugi. 1985. Non-steady motion in unloaded contractions of single frog cardiac cells. *Biophys. J.* 48: 461–465.

Toride, M., and H. Sugi. 1989. Stepwise sarcomere shortening in locally activated frog skeletal muscle fibers. *Proc. Jpn. Acad.* 65:49–52.

Tourovakaya, A., and G. H. Pollack. 1998. Stepwise length changes during stretch in single sarcomeres of single myofibrils. *Biophys. J.* (in press). (Abstr.).

Trinick, J., P. Knight, and A. Whiting. 1984. Purification and properties of native titin. *J. Mol. Biol.* 180:331–356.

Trombitás, K., P. H. W. W. Baatsen, and G. H. Pollack. 1988. I-bands of striated muscle contain lateral struts. *J. Ultrastruct. Mol. Struct. Res.* 100:13–30.

Trombitás, K., G. H. Pollack, J. Wright, and K. Wang. 1993. Elastic properties of titin filaments demonstrated using a "freeze-break" technique. *Cell Motil. Cytoskel.* 24:274–283.

Tskhovrebova, L., J. Trinick, J. Sleep, and R. Simmons. 1997. Elasticity and unfolding of single molecules of the giant muscle protein titin. *Nature.* 387:308–312.

Wang, K., R. McCarter, J. Wright, J. Beverly, and R. Ramirez-Mitchell. 1993. Viscoelasticity of the sarcomere matrix of skeletal muscle. *Biophys. J.* 64:1161–1177.

Wang, S. M., and M. L. Greaser. 1985. Immunocytochemical studies using a monoclonal antibody to bovine cardiac titin on intact and extracted myofibrils. *J. Cell. Biol.* 107:1075–1083.

Zocchi, G. 1997. Proteins unfold in steps. *Proc. Natl. Acad. Sci. USA.* 94:10647–10651.